LETTER

doi:10.1038/nature13436

Tracking photon jumps with repeated quantum non-demolition parity measurements

L. Sun[1]†, A. Petrenko[1], Z. Leghtas[1], B. Vlastakis[1], G. Kirchmair[1]†, K. M. Sliwa[1], A. Narla[1], M. Hatridge[1], S. Shankar[1], J. Blumoff[1], L. Frunzio[1], M. Mirrahimi[1,2], M. H. Devoret[1] & R. J. Schoelkopf[1]

Quantum error correction is required for a practical quantum computer because of the fragile nature of quantum information. In quantum error correction, information is redundantly stored in a large quantum state space and one or more observables must be monitored to reveal the occurrence of an error, without disturbing the information encoded in an unknown quantum state. Such observables, typically multi-quantum-bit parities, must correspond to a special symmetry property inherent in the encoding scheme. Measurements of these observables, or error syndromes, must also be performed in a quantum non-demolition way (projecting without further perturbing the state) and more quickly than errors occur. Previously, quantum non-demolition measurements of quantum jumps between states of well-defined energy have been performed in systems such as trapped ions[1–3], electrons[4], cavity quantum electrodynamics[5,6], nitrogen–vacancy centres[7–9] and superconducting quantum bits[10,11]. So far, however, no fast and repeated monitoring of an error syndrome has been achieved. Here we track the quantum jumps of a possible error syndrome, namely the photon number parity of a microwave cavity, by mapping this property onto an ancilla quantum bit, whose only role is to facilitate quantum state manipulation and measurement. This quantity is just the error syndrome required in a recently proposed scheme for a hardware-efficient protected quantum memory using Schrödinger cat states (quantum superpositions of different coherent states of light) in a harmonic oscillator[12]. We demonstrate the projective nature of this measurement onto a region of state space with well-defined parity by observing the collapse of a coherent state onto even or odd cat states. The measurement is fast compared with the cavity lifetime, has a high single-shot fidelity and has a 99.8 per cent probability per single measurement of leaving the parity unchanged. In combination with the deterministic encoding of quantum information in cat states realized earlier[13,14], the quantum non-demolition parity tracking that we demonstrate represents an important step towards implementing an active system that extends the lifetime of a quantum bit.

As well as being necessary in quantum error correction (QEC) and quantum information, quantum non-demolition (QND) measurements have a central role in quantum mechanics. The application of an ideal projective QND measurement yields a result corresponding to an eigenvalue of the measured operator, and projects the system onto the eigenstate associated with that eigenvalue. Moreover, the measurement must leave the system in that state, so that subsequent measurements always return the same result. The hallmark of a continuously repeated high-fidelity QND measurement is that it demonstrates a canonical thought experiment: individual quantum jumps between eigenstates are resolved in time on a single quantum system. This ideal measurement capability has been experimentally realized only in the past few decades. The jumps of a two-level system (quantum bit, or qubit) between its energy eigenstates were first observed for single trapped ions[1–3], and later in single nitrogen–vacancy centres in diamond[7–9]. The jumps of an oscillator between eigenstates with different numbers of excitations (Fock states), were first observed for the motion of an electron in a Penning trap[4]. More recently, the observation of quantum jumps of light in cavity quantum electrodynamics[5,6] (QED), where the number of microwave photons in a cavity is probed with Rydberg atoms, has enabled a range of new experiments in quantum feedback and control[15,16].

An analogous system to cavity QED is the combination of microwave photons in a superconducting resonator with superconducting qubits, known as circuit QED[17]. The strong dispersive interaction of a qubit and a photon, as in Rydberg-atom cavity QED, allows either the qubit or the cavity to act as a QND probe of the other component. With the advent of quantum-limited parametric amplifiers[18,19], measurement techniques for superconducting devices have rapidly advanced. For instance, the frequency shift of a cavity has recently been used to observe the quantum jumps of a qubit between energy eigenstates[10,11]. So far, however, there have been no observations of jumps for the cavity field in circuit QED. A recent paper measured a different quantity, the parity of two qubits, in a step towards the conventional approach of QEC[20]. However, that work did not present real-time tracking of the jumps due to the natural error rate of that quantity.

In this work, we use the dispersive qubit–cavity interaction of circuit QED to observe the jumps of photon number parity. Importantly, these jumps reveal the loss of individual photons without projecting the system onto a state of definite number or energy, but rather into an eigenspace of even or odd photon number. This characteristic is a crucial requirement for future applications in quantum information, where the parity measurement serves as the error syndrome for correcting a quantum memory. Even in the presence of rapidly repeated measurements, the smooth decay of the ensemble-averaged parity is largely unperturbed. However, when individual time records of the measurement are examined, the parity is observed to take on only the extremal values, ± 1, indicating the projective nature of each individual measurement. On examining the statistics of the jumps recorded over many trajectories, we find excellent agreement with a numerical simulation, suggesting that 85% of the jumps for states with an average photon number $\bar{n} = 4$ are faithfully detected (see Methods section on photon jump statistics). When selecting on the outcome of a single parity measurement, we observe, by Wigner tomography[21], the creation of cat states with $\bar{n}$ up to 4.

In our experiment, we use a three-dimensional circuit QED architecture[22] with a single 'vertical' superconducting transmon qubit (the qualifier 'vertical' indicates that the dominant electric field is perpendicular to the film plane) coupled to two waveguide cavities[14,23], as shown in Fig. 1a. Our qubit has a transition frequency of $\omega_q/2\pi = 5.938$ GHz, an energy relaxation time of $T_1 = 8$ μs and a Ramsey time of $T_2^* = 5$ μs. The high-frequency cavity, with a resonant frequency of $\omega_m/2\pi = 8.174$ GHz and a lifetime of 30 ns, serves only as a fast readout of the qubit state. To perform a high-fidelity single-shot dispersive readout of the qubit, we use a Josephson bifurcation amplifier (JBA) operating in a double-pumped

[1]Departments of Applied Physics and Physics, Yale University, New Haven, Connecticut 06511, USA. [2]INRIA Paris-Rocquencourt, Domaine de Voluceau, BP 105, 78153 Le Chesnay Cedex, France. †Present addresses: Center for Quantum Information, Institute for Interdisciplinary Information Sciences, Tsinghua University, Beijing 100084, China (L.S.); Institut für Experimentalphysik, Universität Innsbruck, Technikerstraße 25, A-6020 Innsbruck, Austria and Institut für Quantenoptik und Quanteninformation, Österreichische Akademie der Wissenschaften, Otto-Hittmair-Platz 1, A-6020 Innsbruck, Austria (G.K.).

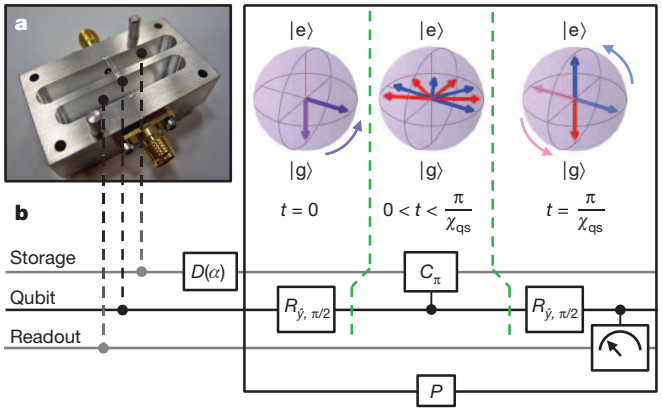

Figure 1 | Experimental device and parity measurement protocol of a photon state. **a**, Bottom half of the device containing a 'vertical' transmon qubit located in a trench and coupled to two waveguide cavities. The low-frequency cavity, with $\omega_s/2\pi = 7.216$ GHz and a lifetime of $\tau_0 = 55$ μs, is used to store and manipulate quantum states. The high-frequency cavity, with $\omega_m/2\pi = 8.174$ GHz and a lifetime of 30 ns, allows for fast readout of the qubit. **b**, Protocol (P) for measuring the parity of the storage cavity field. After an initial displacement of cavity vacuum $D(\alpha)|0\rangle = |\alpha\rangle$ to create a coherent state with a complex amplitude α, a Ramsey-type measurement is performed. It consists of two π/2-pulses separated by $t = \pi/\chi_{qs}$ (during which a controlled-phase gate $C_\pi = I\otimes|g\rangle\langle g| + e^{i\pi a^\dagger a}\otimes|e\rangle\langle e|$ is realized), followed by a projective measurement of the qubit, where χ_{qs} is the dispersive interaction between the qubit and the storage cavity. In this schematic, with the qubit initially in the ground state, $|g\rangle$, the Ramsey-type measurement maps the even and odd photon states onto the $|e\rangle$ and $|g\rangle$ states of the qubit, respectively. A subsequent projective measurement indicates the cavity state parity. The second π/2-pulse can be either $R_{\hat{y},-\pi/2}$ or $R_{\hat{y},\pi/2}$, simply switching the interpretation of the result of the qubit measurement.

mode[24,25] as the first stage of amplification. The low-frequency cavity, with a resonant frequency of $\omega_s/2\pi = 7.216$ GHz and a lifetime of $\tau_0 = 55$ μs, stores the photon states which are measured and manipulated. Exploiting the nonlinearities induced in both resonators, we use the transmon qubit to track the parity of the storage cavity state. For simplicity, we will refer to the storage cavity as the 'cavity' henceforth.

The qubit and cavity are in the regime of strong dispersive coupling, which can be described by the Hamiltonian

$$H/\hbar = \omega_q|e\rangle\langle e| + \left(\omega_s - \chi_{qs}|e\rangle\langle e|\right)a^\dagger a$$

where a and $a^\dagger$ are the annihilation and creation operators, respectively, $|e\rangle$ is the excited state of the qubit and $\chi_{qs}/2\pi = 1.789$ MHz is the qubit-state-dependent frequency shift of the cavity. The readout cavity has been neglected because it remains in the ground state while the system evolves. The interaction between the qubit and the cavity entangles qubit and photon. In the rotating frame of the cavity, Fock states associated with the qubit in the excited state acquire a phase $\Phi = a^\dagger a\chi_{qs}t$ proportional to their photon number[26]. By waiting for $t = \pi/\chi_{qs}$, one can realize a controlled-phase gate $C_\pi = I\otimes|g\rangle\langle g| + e^{i\pi a^\dagger a}\otimes|e\rangle\langle e|$, where $|g\rangle$ is the ground state of the qubit, adding a phase shift of π per photon to the cavity state conditioned on the qubit state[14,27]. Therefore, C_π can be inserted between two π/2-pulses on the qubit in a Ramsey-type measurement to map the photon parity of any cavity state onto the qubit (black enclosure labelled 'P' in Fig. 1b). The result of a qubit measurement after the second π/2-pulse, together with prior knowledge of the initial qubit state, indicates whether the number of photons in the cavity is even or odd, but reveals nothing about the actual value of the photon number.

The creation of cat states is a natural consequence of a parity measurement on a coherent state $|\alpha\rangle$ (α is a complex amplitude) because the phase cat states defined by $\mathcal{N}_\pm(|\alpha\rangle \pm |-\alpha\rangle)$, with $\mathcal{N}_\pm = 1/\sqrt{2\left(1 \pm e^{-2|\alpha|^2}\right)}$, are eigenstates of the parity operator $e^{i\pi a^\dagger a}$ (refs 28, 29). After applying a microwave pulse at frequency ω_s to the cavity, initially in vacuum, to create a coherent state $|\alpha\rangle$ with the qubit initially in $|g\rangle$, we use the parity protocol to take $|\alpha\rangle(|g\rangle + |e\rangle)/\sqrt{2}$ after the first π/2-pulse to $[\mathcal{N}_-(|\alpha\rangle - |-\alpha\rangle)|g\rangle + \mathcal{N}_+(|\alpha\rangle + |-\alpha\rangle)|e\rangle]/\sqrt{2}$ after the second pulse, at which point the parity of the cavity state is entangled with the state of the qubit. Detection of the qubit state using the readout cavity then projects the storage cavity onto one of the two cat states. To confirm the non-classical properties of these states, we perform Wigner tomography of the cavity after a single parity measurement for an initial coherent state of displacement $|\alpha| = 2$ ($\bar{n} = 4$). Post-selecting on the ground or excited qubit states to obtain the odd or even cats (Fig. 2a, b), respectively, we see the interference patterns that are the signature of quantum behaviour. The overlap between the measured Wigner function and that of an ideal cat state gives a fidelity of $F = 83\%$ for the odd cat state. Figure 2c shows the Wigner function without post-selection (tracing over qubit states). Fringes in the Wigner function almost completely disappear, as expected, and we obtain the statistical mixture of even and odd states. The weak visibility of the fringes comes from the slightly lower fidelity of the even cat state, wherein the qubit ends up in the $|e\rangle$ state, which is more susceptible to qubit relaxation. Figure 2d shows the normalized difference between the two cat states to emphasize the interference fringes. The high contrast between even and odd cat states is a central requirement in implementing a recently proposed QEC scheme[12], where these form the code and error spaces, respectively.

Because the loss of a single photon changes the parity of a cat state, monitoring parity repeatedly in real time allows us to track photon jumps of our cavity. Here we note that to interpret the result of a single parity measurement we must know the state of the qubit before the first π/2-pulse. In other words, it is the correlation of the qubit states before and after the parity measurement (a pattern of oscillation between $|g\rangle$ and $|e\rangle$ versus a constant pattern remaining in either $|g\rangle$ or $|e\rangle$) that reveals the photon state parity. For the following data we have chosen $R_{\hat{y},-\pi/2}$ as the second qubit pulse, instead of $R_{\hat{y},\pi/2}$, to maintain a constant pattern when the cavity is in the even parity state. Apart from reversing which pattern we assign to be even and which we assign to be odd, this change makes no difference. Figure 3a shows the measurement protocol and Fig. 3b–e shows typical 400 μs single-shot traces. The initial displacement is $|\alpha| = 1.0$ and the repetition interval of the parity measurements is 1 μs, which is much smaller than the average photon lifetime, $\tau_0 = 55$ μs,

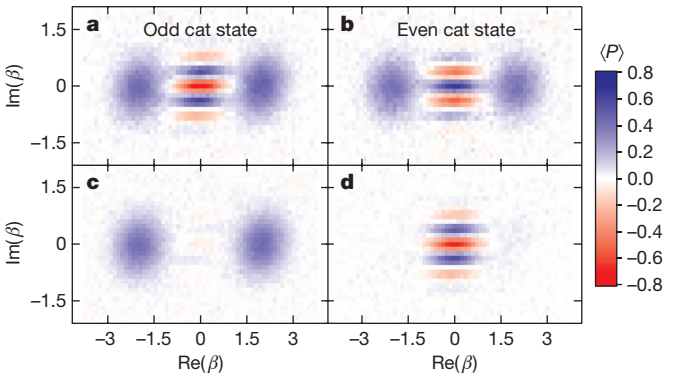

Figure 2 | Ensemble-averaged Wigner functions of cat states in the cavity created by single-shot parity measurements of an initial coherent state in the cavity. The Wigner functions are mapped out with varying displacements β and a measurement of the mean photon parity $\langle P\rangle$ (ref. 21). Here we follow the protocol depicted in Fig. 1b, using $R_{\hat{y},\pi/2}$ as the second pulse. The qubit is always initialized to the $|g\rangle$ state through post-selection on an initial measurement. **a**, Odd cat state by post-selection on the $|g\rangle$ state as the result of the parity measurements. **b**. Even cat state by post-selection on the $|e\rangle$ state. **c**, No post-selection of the parity measurement, thus tracing over the qubit state. Fringes almost disappear, indicating a mixture of two coherent states. **d**, The normalized difference (data in **a** minus data in **b**, all divided by two), or the expectation of the parity weighted by $\langle\sigma_z\rangle$ of the ancilla, emphasizing the interference fringes.

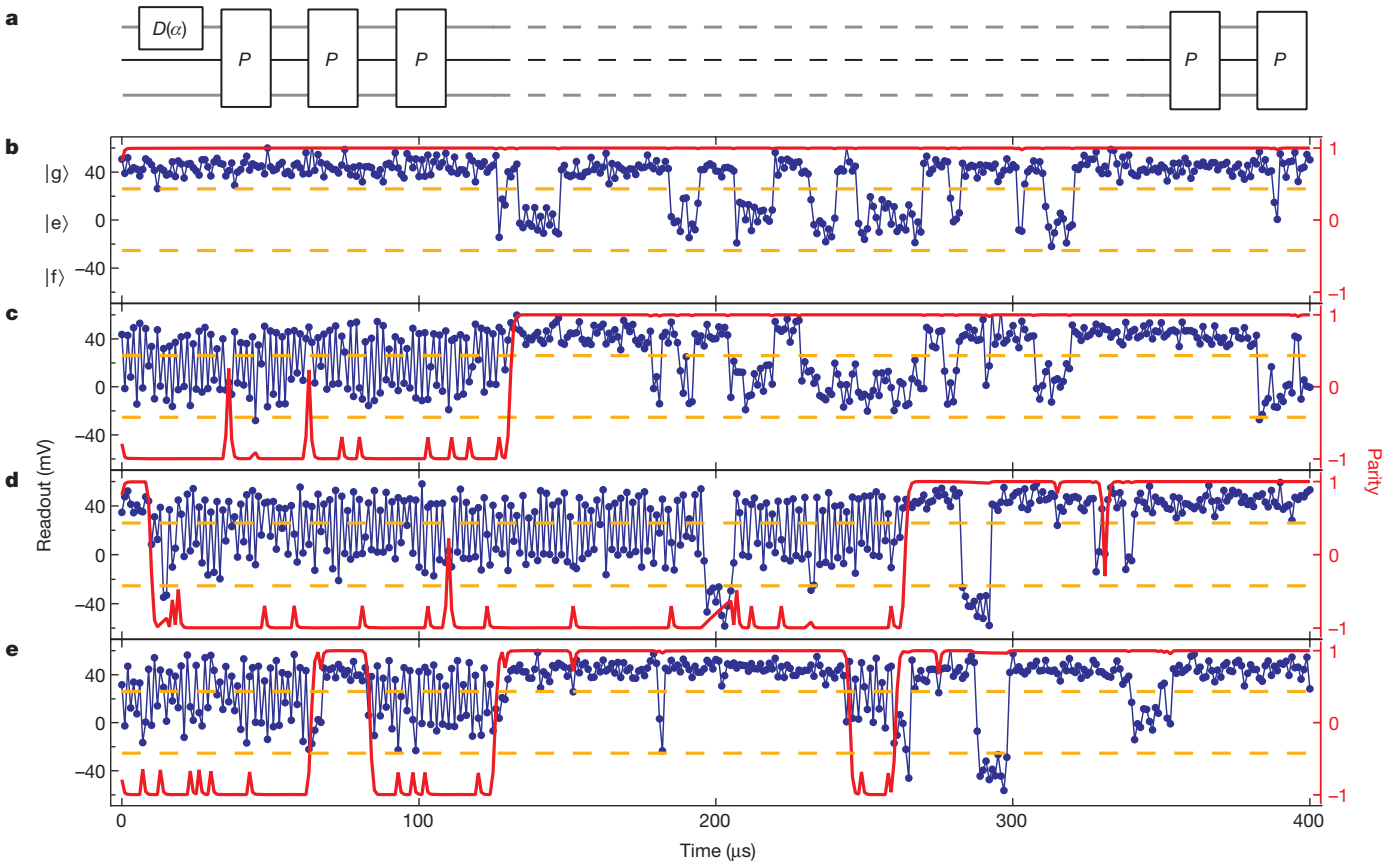

Figure 3 | Typical repeated single-shot parity measurement traces revealing photon jumps in real time. Horizontal dashed orange lines delineate the thresholds to distinguish $|g\rangle$, $|e\rangle$ and higher excited states of the qubit, denoted as $|f\rangle$. The red traces show the quantum filter that best estimates the parity at every point. The filter has a finite response time and thus does not trust that a brief change in the measurement pattern corresponds to an actual parity jump. **a**, In this protocol we switch the sign of the second pulse, using $R_{\hat{y},-\pi/2}$ instead of $R_{\hat{y},\pi/2}$. The repetition time of the parity measurement is 1 μs, and the traces in **b**–**e** all have an initial displacement of $|\alpha| = 1$. **b**, For the most part, the correlation between neighbouring measurements is positive, indicating an even-parity state for the whole 400 μs. The changes in the qubit state between 120 μs and 320 μs are probably due to qubit decoherence during the parity measurement. **c**, One parity jump is observed by the change in the measurement pattern (oscillating versus constant) at about 130 μs. **d**, Two parity jumps are recorded at about 10 μs and then again at 260 μs. The change of pattern at about 200 μs is a result of the qubit leaving the computational space for higher excited states, a feature that disables the parity measurement until the qubit returns to either $|g\rangle$ or $|e\rangle$. **e**, A trace with all features described above included. In this particular trajectory, the filter can clearly resolve five photon jump events.

obtained from a free time evolution measurement of the parity of a coherent state (see Methods section on experimental set-up). We observe a range of photon jump statistics, from quiet traces that last for hundreds of microseconds with no apparent changes in parity, to those that have as many as five jumps. The clear dichotomy between the patterns in our traces indicates that, although the measurements are susceptible to qubit decoherence, as evidenced by intermittent, brief changes in measurement correlations and excitations to higher qubit states, they nonetheless exhibit a strong sensitivity to single-photon jump events.

When analysing these single-shot traces, to mitigate the effects due to qubit decoherence, excitation to qubit states higher than $|e\rangle$ (denoted as $|f\rangle$) and other imperfections in the qubit readout in extracting the parity, we have applied a quantum filter that best estimates the photon state parity (see Methods section on the quantum filter). We note that the output of the quantum filter depends on the entire previous parity trajectory. Figure 3b–e shows traces with the parity estimator calculated from the quantum filter, in red. The parity estimator is clearly much less sensitive to qubit decoherence and $|f\rangle$ states. Although our single parity readout fidelity is 80%, owing to the smoothing effect of the quantum filter we actually can achieve nearly unity detection sensitivity of single-photon jumps. However, given one jump, the probability of there being a second jump within the response time of the filter (~2 μs) is 4% for $\bar{n} = 1$ (or 15% for $\bar{n} = 4$), which limits our overall detection sensitivity over an entire trajectory (see Methods section on photon jump statistics).

The repeated parity measurements shown above constitute just a single point, the origin, in the Wigner functions of the even and odd cat states (Fig. 2a, b). Thus, crucially, a parity measurement acquires no information about the phase of the cat states. Consequently, one could encode quantum information onto the computational bases $|0\rangle_L = \mathcal{N}_+(|\alpha\rangle + |-\alpha\rangle)$ and $|1\rangle_L = \mathcal{N}_+(|i\alpha\rangle + |-i\alpha\rangle)$, and any subsequent parity measurements would make no distinction between the two. The loss of a single photon will change the code space spanned by $|0\rangle_L$ and $|1\rangle_L$ into the error space spanned by $|\bar{0}\rangle_L = \mathcal{N}_-(|\alpha\rangle - |-\alpha\rangle)$ and $|\bar{1}\rangle_L = \mathcal{N}_-(|i\alpha\rangle - |-i\alpha\rangle)$ with a different parity. This error syndrome can thus be extracted by the parity measurement demonstrated here, but without gaining any knowledge of the information encoded in the cat states, as required by QEC.

The degree to which the measurements are QND can be determined by examining the decay rate for the parity of a coherent state with different measurement cadences. We extract the total decay rate of the parity (τ_{tot}), from the ensemble-averaged parity dynamics obtained with the quantum filter (Fig. 4). This total decay rate is well modelled by the parallel combination of the free decay time ($\tau_0 = 55$ μs) plus a constant demolition probability $P_D = 0.002$ per measurement interval τ_i, as shown by the fit in the inset of Fig. 4. In other words, a single parity measurement is 99.8% QND, leaving the parity of the cavity state largely unperturbed.

Several improvements and further investigations will be required to realize a truly robust error-corrected quantum memory. The probability of missing a photon jump, as a result of the finite measurement rate

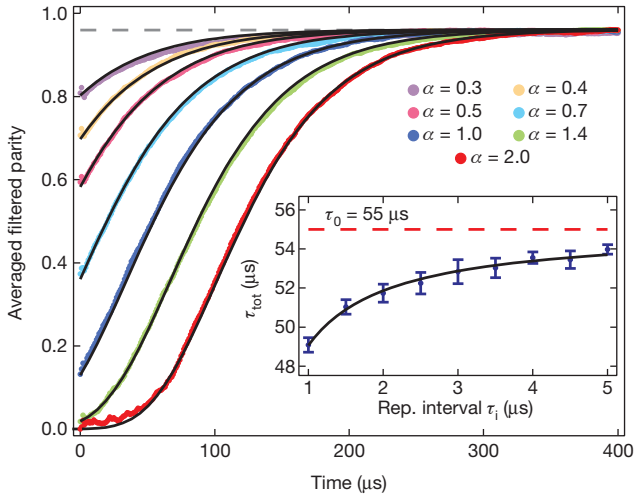

Figure 4 | Ensemble average of filtered single-shot parity traces for different cavity displacements α. The $|\alpha| = 1$ curve is the average of 20,000 traces, the examples of which are shown in red in Fig. 3b–e. Note that there is no post-selection on the initial parity of the cat state. Parity measurements are repeated every $\tau_i = 1$ μs. The parity of an initial coherent state is expected to evolve as $P = e^{-2|\alpha|^2 e^{-t/\tau_{tot}}}/(1+2n_{th})/(1+2n_{th})$, where τ_{tot} is the photon decay time and n_{th} is the background photon number in the cavity (see Methods section on the quantum filter). Given $n_{th} = 0.02$ (from an independent measurement; see Methods section on the experimental set-up), the average parity is expected to saturate at $1/(1+2n_{th}) = 0.96$ (the dashed horizontal line). Solid lines are fitted theoretical curves for coherent states where n_{th} and the corresponding $|\alpha|$ are fixed, leaving τ_{tot} as the only free parameter. Here the value of $\tau_{tot} = 49$ μs gained from a global fit closely matches the lifetime $\tau_0 = 55$ μs obtained from free evolution, and each trace indeed saturates at $P = 0.96$. This indicates that repeated parity measurements do not significantly perturb the cavity state, inducing neither extra jumps nor an increase in cavity thermal population. Inset, extracted time constants as functions of different parity measurement repetition intervals. The error bars indicate one standard deviation calculated from nine measurements, as in the main panel. The decay time τ_{tot} is modelled as $1/\tau_{tot} = 1/\tau_0 + P_D/\tau_i$, where P_D is the probability of inducing an extra parity change. A fit (solid line) gives $P_D = 2 \times 10^{-3}$, indicating that a single parity measurement is 99.8% QND.

per cavity lifetime, would be greatly reduced if longer-lived cavities were used[30]. It is a necessary, but not sufficient, condition that the measurement itself, as shown here, is highly QND and unlikely to induce photon jumps. An additional requirement is that the measurement does not destroy the actual quantum information stored in the cat states. Dephasing of the cavity state will be non-negligible because the current realization is not yet robust against qubit decay or excitation (see Methods section on quantifying the parity-tracking performance). Increasing qubit and cavity lifetimes, and further characterizing these types of error processes, are important next steps. Nonetheless, we estimate that when combined with an optimized measurement strategy, the current level of performance could already allow extension of the average lifetime of an encoded cat state ($\tau_{tot}/\bar{n}$) by a factor of two (see Methods section on parity-tracking performance). There are several other theoretical architectures for QEC, some of which have already been implemented experimentally. However, these experiments have not yet reached the level where they can suppress the naturally occurring errors. Understanding the role of the measurement process and its imperfections in all of these approaches remains an important topic for current and future work.

We have demonstrated the real-time tracking of jumps in the photon number parity in circuit QED. Significantly, this quantity differs from previous observations of quantum jumps between energy levels. Rather, it projects the system into a degenerate subspace, and can therefore serve as an error syndrome for QEC. We show that the parity measurement is highly QND and that it has a high fidelity and cadence compared with the cavity lifetime. These advances in the measurement capabilities should enable further progress in quantum information.

METHODS SUMMARY

Measurements are performed in a cryogen-free dilution refrigerator with a base temperature of about 10 mK. The 'vertical' transmon qubit is fabricated on a *c*-plane sapphire (Al_2O_3) substrate with a double-angle evaporation of aluminium after a single electron-beam lithography step. The state-dependent frequency shift between the qubit and the readout cavity is $\chi_{qr}/2\pi = 0.930$ MHz, which is not optimized for the best signal-to-noise ratio. The background photon number $n_{th} = 0.02$ and the displacement α are calibrated on the basis of the Poisson distribution of photon numbers in the storage cavity (Extended Data Fig. 2). The qubit readout fidelity is about 90%, mainly limited by the short coherence times of the qubit. The quantum filter used as the best-parity estimator consists of two steps: a time evolution of the density matrix taking into account the cavity decoherence, and a modification of the density matrix based on the current measurement result. The effectiveness of this filter is confirmed by the good agreement between extracted numbers of jumps from the parity estimator during 500 μs repeated parity measurements and a numerical simulation (Extended Data Fig. 9). The Wigner tomography fidelity is limited by qubit T_1, T_ϕ, photon jumps and detection inaccuracy. Among these factors, only qubit T_1 and missing of fast photon jumps can lead to the decay of the cat states. The high-QND nature of the parity measurement allows the incorrect parity measurement result due to qubit T_ϕ and detection inaccuracy to be removed by performing repeated parity measurements and taking a majority voting. Slow photon jumps can be tracked as demonstrated in the manuscript, and the resulting phase errors of the cat states can also be completely corrected. Repeated parity tracking can thus enhance the lifetime of the information encoded in cat states (Methods section on parity-tracking performance).

Online Content Methods, along with any additional Extended Data display items and Source Data, are available in the online version of the paper; references unique to these sections appear only in the online paper.

Received 12 November 2013; accepted 6 May 2014.
Published online 13 July 2014.

1. Bergquist, J. C., Hulet, R. G., Itano, W. M. & Wineland, D. J. Observation of quantum jumps in a single atom. *Phys. Rev. Lett.* **57,** 1699–1702 (1986).
2. Sauter, T., Neuhauser, W., Blatt, R. & Toschek, P. E. Observation of quantum jumps. *Phys. Rev. Lett.* **57,** 1696–1698 (1986).
3. Nagourney, W., Sandberg, J. & Dehmelt, H. Shelved optical electron amplifier: observation of quantum jumps. *Phys. Rev. Lett.* **56,** 2797–2799 (1986).
4. Peil, S. & Gabrielse, G. Observing the quantum limit of an electron cyclotron: QND measurements of quantum jumps between Fock states. *Phys. Rev. Lett.* **83,** 1287–1290 (1999).
5. Gleyzes, S. *et al.* Quantum jumps of light recording the birth and death of a photon in a cavity. *Nature* **446,** 297–300 (2007).
6. Guerlin, C. *et al.* Progressive field-state collapse and quantum non-demolition photon counting. *Nature* **448,** 889–893 (2007).
7. Jelezko, F. *et al.* Single spin states in a defect center resolved by optical spectroscopy. *Appl. Phys. Lett.* **81,** 2160–2162 (2002).
8. Neumann, P. *et al.* Single-shot readout of a single nuclear spin. *Science* **329,** 542–544 (2010).
9. Robledo, L. *et al.* High-fidelity projective read-out of a solid-state spin quantum register. *Nature* **477,** 574–578 (2011).
10. Vijay, R., Slichter, D. H. & Siddiqi, I. Observation of quantum jumps in a superconducting artificial atom. *Phys. Rev. Lett.* **106,** 110502 (2011).
11. Hatridge, M. *et al.* Quantum back-action of an individual variable-strength measurement. *Science* **339,** 178–181 (2013).
12. Leghtas, Z. *et al.* Hardware-efficient autonomous quantum error correction. *Phys. Rev. Lett.* **111,** 120501 (2013).
13. Leghtas, Z. *et al.* Deterministic protocol for mapping a qubit to coherent state superposition in a cavity. *Phys. Rev. A* **87,** 042315 (2013).
14. Vlastakis, B. *et al.* Deterministically encoding quantum information using 100-photon Schrödinger cat states. *Science* **342,** 607–610 (2013).
15. Deléglise, S. *et al.* Reconstruction of non-classical cavity field states with snapshots of their decoherence. *Nature* **455,** 510–514 (2008).
16. Sayrin, C. *et al.* Real-time quantum feedback prepares and stabilizes photon number states. *Nature* **477,** 73–77 (2011).
17. Devoret, M. H. & Schoelkopf, R. J. Superconducting circuits for quantum information: an outlook. *Science* **339,** 1169–1174 (2013).
18. Castellanos-Beltran, M. A., Irwin, K. D., Hilton, G. C., Vale, L. R. & Lehnert, K. W. Amplification and squeezing of quantum noise with a tunable Josephson metamaterial. *Nature Phys.* **4,** 929–931 (2008).
19. Bergeal, N. *et al.* Phase-preserving amplification near the quantum limit with a Josephson ring modulator. *Nature* **465,** 64–68 (2010).
20. Ristè, D. *et al.* Deterministic entanglement of superconducting qubits by parity measurement and feedback. *Nature* **502,** 350–354 (2013).
21. Haroche, S. & Raimond, J. M. *Exploring the Quantum: Atoms, Cavities, and Photons* (Oxford Univ. Press, 2006).
22. Paik, H. *et al.* Observation of high coherence in Josephson junction qubits measured in a three-dimensional circuit QED architecture. *Phys. Rev. Lett.* **107,** 240501 (2011).
23. Kirchmair, G. *et al.* Observation of quantum state collapse and revival due to the single-photon Kerr effect. *Nature* **495,** 205–209 (2013).

24. Kamal, A., Marblestone, A. & Devoret, M. H. Signal-to-pump back action and self-oscillation in double-pump Josephson parametric amplifier. *Phys. Rev. B* **79,** 184301 (2009).
25. Murch, K. W., Weber, S. J., Macklin, C. & Siddiqi, I. Observing single quantum trajectories of a superconducting quantum bit. *Nature* **502,** 211–214 (2013).
26. Schuster, D. I. *et al.* Resolving photon number states in a superconducting circuit. *Nature* **445,** 515–518 (2007).
27. Bertet, P. *et al.* Direct measurement of the Wigner function of a one-photon Fock state in a cavity. *Phys. Rev. Lett.* **89,** 200402 (2002).
28. Brune, M., Haroche, S., Raimond, J. M., Davidovich, L. & Zagury, N. Manipulation of photons in a cavity by dispersive atom-field coupling: Quantum-nondemolition measurements and generation of ''Schrödinger'' cat states. *Phys. Rev. A* **45,** 5193–5214 (1992).
29. Brune, M. *et al.* Observing the progressive decoherence of the ''meter'' in a quantum measurement. *Phys. Rev. Lett.* **77,** 4887–4890 (1996).
30. Reagor, M. *et al.* Ten milliseconds for aluminum cavities in the quantum regime. *Appl. Phys. Lett.* **102,** 192604 (2013).

Acknowledgements We thank L. Jiang and S. M. Girvin for discussions. Facilities use was supported by the Yale Institute for Nanoscience and Quantum Engineering and the US NSF MRSEC DMR 1119826. This research was supported in part by the Office of the Director of National Intelligence (ODNI), Intelligence Advanced Research Projects Activity (IARPA), through the Army Research Office (W911NF-09-1-0369) and in part by the US Army Research Office (W911NF-09-1-0514). All statements of fact, opinion or conclusions contained herein are those of the authors and should not be construed as representing the official views or policies of IARPA, the ODNI or the US government. M.M. acknowledges partial support from the Agence National de Recherche under the project EPOQ2, ANR-09-JCJC-0070. B.V. acknowledges partial support from NSF under the project PHY-1309996.

Author Contributions L.S. and A.P. performed the experiment and analysed the data. Z.L. and M.M. provided theoretical support. B.V. and G.K. provided further experimental contributions. K.M.S., A.N., M.H. and S.S. contributed to the double-pumped Josephson bifurcation amplifier under the supervision of M.H.D. J.B. and L.F. fabricated the device. R.J.S. designed and supervised the project. L.S., A.P., L.F. and R.J.S. wrote the manuscript with feedback from all authors.

Author Information Reprints and permissions information is available at www.nature.com/reprints. The authors declare no competing financial interests. Readers are welcome to comment on the online version of the paper. Correspondence and requests for materials should be addressed to L.S. (luyansun@mail.tsinghua.edu.cn) or R.J.S. (robert.schoelkopf@yale.edu).

METHODS

Experiment set-up, device parameters and qubit readout properties. Our measurements are performed in a cryogen-free dilution refrigerator with a base temperature of about 10 mK. Extended Data Fig. 1 shows the schematic of the measurement set-up. A Josephson bifurcation amplifier[31,32] (JBA) operating in a double-pumped mode[24,25] is used as the first stage of amplification between the readout cavity output and the high-electron-mobility transistor (HEMT), allowing for a high-fidelity single-shot dispersive readout of the qubit state. We typically operate the JBA in the saturated regime with about 20 readout photons for a better signal-to-noise ratio.

The 'vertical' transmon qubit is fabricated on a *c*-plane sapphire (Al_2O_3) substrate with a double-angle evaporation of aluminium after a single electron-beam lithography step. We use the word 'vertical' to specify that the dominant electric field is perpendicular to the film plane. The qubit has a transition frequency $\omega_q/2\pi = 5.938$ GHz with an anharmonicity of $\alpha_q/2\pi = (\omega_{ge} - \omega_{ef})/2\pi = 240$ MHz, an energy relaxation time of $T_1 = 8$ μs and a Ramsey time of $T_2^* = 5$ μs. These coherence times are short compared with those in a regular three-dimensional cavity[22], but are comparable to those reported in refs 14, 23. Exploring the exact sources of limitation is an on-going research subject. Even at the lowest base temperature, the qubit steady state is measured to be a thermal mixture of about 86% ground state $|g\rangle$, 11% excited state $|e\rangle$ and 3% states higher than $|e\rangle$, denoted as $|f\rangle$. These excitations of the qubit could come from stray infrared photons leaking into the cavity, although the exact source remains unknown.

The qubit serves as an ancilla and provides the necessary nonlinearity for the manipulation of coherent states in the storage cavity. Both the storage and readout cavities are made of aluminium alloy 6061. The state-dependent frequency shifts between the qubit and the storage and readout cavities are $\chi_{qs}/2\pi = 1.789$ MHz and $\chi_{qr}/2\pi = 0.930$ MHz, respectively. For simplicity, we will refer to the storage cavity as the 'cavity' henceforth. The inset of Extended Data Fig. 2 shows the 'number splitting peaks' of the qubit due to different photon numbers in the cavity, which is displaced with a 10 ns square pulse right before the spectroscopy measurement. A second-order polynomial fit $\chi(n) = -\chi_{qs}n + \chi'_{qs}n^2$, where n is the peak number, gives a nonlinear correction to the dispersive shift[14] $\chi'_{qs}/2\pi = 1.9 \pm 0.1$ kHz which is small enough to be neglected in the cavity dynamics. Extended Data Fig. 2 shows that the probabilities of the first eight Fock states $n = 0, 1, 2, \ldots, 7$ as functions of displacement amplitude $|\alpha|$ are in excellent agreement with a Poisson distribution, indicating good control of the coherent state in the cavity. We scale the x axis from the voltage amplitude of the displacement pulse applied from an arbitrary waveform generator and use this scaling as a calibration. There is a small residual amplitude for the $n = 1$ peak even with no displacement (point near origin), allowing us to infer that there is a background photon population $n_{th} = 0.02$ in the cavity. The lifetime of the cavity is characterized by measuring a free parity evolution of a coherent state, as shown in Extended Data Fig. 3, which is nearly identical to Fig. 4. A global fit gives a time constant $\tau_0 = 55$ μs. We also perform another experiment by introducing a small average photon number ($\bar{n} \approx 0.1$) in the cavity and monitoring the exponential decay of the $n = 1$ qubit peak. This experiment gives an identical τ_0. However, the free parity evolution of a coherent state can have much better signal-to-noise ratio because large $\bar{n}$ (as large as 4) can be introduced in the cavity.

To perform a good parity measurement, the π/2-pulses $R_{\hat{y},\pm\pi/2}$ should equally cover as many number splitting peaks as possible without significantly exciting the $|f\rangle$ state. We choose a Gaussian envelope pulse truncated to $4\sigma = 8$ ns ($\sigma_f = 80$ MHz) for a good compromise. Extended Data Fig. 4 shows the effectiveness of those $R_{\hat{y},\pm\pi/2}$ pulses as a function of $\bar{n}$ in the cavity. The curvature for $\bar{n} > 4$ is due to the finite bandwidth of those pulses in the frequency domain.

We have adjusted the phase between the JBA readout signal and the pump such that $|g\rangle$, $|e\rangle$ and $|f\rangle$ states can be distinguished with optimal contrast. Extended Data Fig. 5a shows the histogram of the qubit readout for the parity protocol used in repeated single-shot traces in Fig. 3. The histogram is clearly trimodal. Thresholds between $|g\rangle$ and $|e\rangle$, and between $|e\rangle$ and $|f\rangle$ states, have been chosen to digitize the readout signal to +1, −1 and 0 for $|g\rangle$, $|e\rangle$ and $|f\rangle$ states, respectively. We assign a zero to the $|f\rangle$ states to indicate a 'failed' measurement with no useful information about the parity. These $|f\rangle$ states can be fixed with a field-programmable gate array applying proper pulses to drive the qubit back to either $|g\rangle$ or $|e\rangle$ in real time. Extended Data Fig. 5e shows the basic qubit readout properties with the cavity left in vacuum. The $|g\rangle$ state is prepared through a post-selection of an initial qubit measurement, while $|e\rangle$ and $|f\rangle$ are prepared by properly pulsing the selected $|g\rangle$ state (see Extended Data Fig. 5b–d for the pulse sequences). The loss of fidelity predominantly comes from the T_1 process during both the waiting time of the initialization measurement (500 ns) and the qubit readout time (300 ns).

Wigner tomography fidelity and parity readout fidelity. We emphasize that it is the correlation C_t of the qubit states before and after the parity measurement that reveals the photon state parity. Extended Data Fig. 6a shows the parity readout properties of our system for the protocol ($R_{\hat{y},-\pi/2}$ as the second qubit pulse) used in the single-shot traces in Fig. 3. The loss of fidelity of the parity measurement mainly comes from qubit decoherence processes during the parity measurement (discussed later). Conditional probabilities P(+1|even), P(+1|odd), P(−1|even), P(−1|odd), P(0|even) and P(0|odd) are time-independent probabilities that have positive, negative and zero correlations (as indicated) between the digitized qubit readouts before and after a parity measurement for a given even or odd state. However, a pure even or odd state cannot be prepared easily in our system owing to the finite thermal population of the cavity, which is small but can still introduce systematic errors. We determine P(±1,0|even/odd) by post-selecting the cases with five consecutive identical parity results, which give the photon state parity with good confidence, and then performing a histogram on the sixth parity measurement (Extended Data Fig. 6b).

Extended Data Fig. 6c shows the pulse sequence for producing the cat states and the Wigner tomography shown in Fig. 2. The protocol starts with a post-selection of the $|g\rangle$ state of the qubit after an initial qubit measurement M_1. A parity measurement is performed immediately after a storage cavity displacement α, followed by Wigner tomography with varying displacements β. A 280 ns waiting time after each measurement has been chosen to ensure that the readout cavity returns to the vacuum state. The qubit pulses have a Gaussian envelope truncated to $4\sigma = 8$ ns, and the displacement pulses on the storage cavity are 10 ns square pulses. The dashed enclosures represent the pulse sequence for a parity measurement.

To remove the cross-Kerr effect between the readout cavity and the storage cavity which skews the readout signal for large storage cavity displacements, and also to convert the readout voltage to parity, we followed the procedure in the supplementary material of ref. 14. The idea is to perform two parity measurements of different protocols ($R_{\hat{y},\pi/2}$ or $R_{\hat{y},-\pi/2}$ as the second π/2-pulse) for a vacuum state in the cavity. The difference between the two measurements corresponds to a parity value $P = 1$. We used this technique earlier in Extended Data Fig. 3 and here in the Wigner tomography in Extended Data Fig. 6c.

Extended Data Fig. 6d shows the error budgets for the Wigner tomography fidelity in Fig. 2. The fidelity is defined by the overlap between the measured Wigner state and that of an ideal cat state. We mainly consider qubit T_1, T_ϕ and photon jump processes. First of all, the qubit T_1 and T_ϕ processes and $|f\rangle$ states during Wigner tomography have been included in the parity calibration. After measurement M_1, we post-select only the $|g\rangle$ state of the qubit. Therefore, the system's initial state before the first parity measurement P_1 (note that $R_{\hat{y},\pi/2}$ is the second π/2-pulse) is $|\psi_i\rangle = |\alpha\rangle|g\rangle$. The rotating frame has been fixed to be the one rotating at the cavity frequency ω_s when the qubit is in the $|g\rangle$ state. The qubit T_1 process between the two π/2-pulses in P_1 leads to $|\psi_f\rangle = \left|\alpha e^{i\chi_{qs}t}\right\rangle(|g\rangle + |e\rangle)/\sqrt{2}$, where t is the time of the T_1 jump happening. On average, this process gives 3% fidelity error. The qubit T_ϕ process between the two π/2-pulses in P_1 leads to $|\psi_f\rangle = [\mathcal{N}_+(|\alpha\rangle + |-\alpha\rangle)|g\rangle + \mathcal{N}_-(|\alpha\rangle - |-\alpha\rangle)|e\rangle]/\sqrt{2}$ right before measurement M_2, switching the entanglement relationship between the cat states and the qubit states and causing a full error. Here $\mathcal{N}_\pm = 1/\sqrt{2\left(1 \pm e^{-2|\alpha|^2}\right)}$. Because in our experiment we mainly consider $|\alpha| = 2$, for reasons of simplicity, we use the approximation $\mathcal{N}_+ = \mathcal{N}_- = 1/\sqrt{2}$ in the large-$|\alpha|$ limit in what follows. The photon jump process between the two π/2-pulses in P_1 leads to $|\psi_f\rangle = \left[\left(|\alpha\rangle - e^{i\chi_{qs}t}|-\alpha\rangle\right)|g\rangle + \left(|\alpha\rangle + e^{i\chi_{qs}t}|-\alpha\rangle\right)|e\rangle\right]/2$, where t is the time of the photon jump event happening. On average, in this case the fidelity to the ideal even/odd cat states is 50%. If the photon jump process happens during measurement M_2 and the following waiting time, it switches between the even and odd cat states, thus causing a full error. If the photon jump process happens between the two π/2-pulses during the Wigner tomography, the results in the two parity protocols cancel out on average, leading to a full error as well. Finally, the qubit measurement inaccuracy due to the finite overlap between measurement histograms in P_1 plus the qubit transition up process during the waiting time right after the readout is about 1.3%. The sum of all sources of error limits the Wigner tomography fidelity $F = 84\%$ of the created cat states, consistent with the measurement. To create the even cat state, the measurement M_2 projects the qubit onto the $|e\rangle$ state. The extra qubit T_1 process after the projection lowers its creation fidelity by 280 ns/8 μs = 3.5%. This difference explains the imperfect cancellation of the fringes in Fig. 2c.

Similarly, the error budgets for the parity readout fidelity with $R_{\hat{y},-\pi/2}$ as the second qubit pulse (Extended Data Fig. 6a) can also be estimated, as shown in Extended Data Fig. 6e. We again mainly consider qubit T_1, T_ϕ, $|f\rangle$ state and photon jump processes. We examine the case with the system initially in the state $|\psi_i\rangle = (|\alpha\rangle + |-\alpha\rangle)|g\rangle/\sqrt{2}$ (post-selected by the first five parity measurements), and consider the probability of not measuring the $|g\rangle$ state in the sixth parity measurement. In this case, the qubit T_1 process between the two π/2-pulses has a 50% chance of causing an error. The photon jump process between the two π/2-pulses leads to $|\psi_f\rangle = (|\alpha\rangle - |-\alpha\rangle)\left[\left(1 - e^{i\chi_{qs}t}\right)|g\rangle - \left(1 + e^{i\chi_{qs}t}\right)|e\rangle\right]/2\sqrt{2}$, where t is the time of the photon jump event happening, on average also giving a 50% chance of a wrong answer. The qubit T_ϕ process between the two π/2-pulses flips the qubit

state on the equator of the Bloch sphere and leads to $|\psi_f\rangle = (|\alpha\rangle + |-\alpha\rangle)|e\rangle/\sqrt{2}$, giving a full error in the final readout. Finally, the qubit measurement inaccuracy in the fifth parity measurement plus the qubit transition up process during the waiting time is 1.3%, as in the case of the Wigner tomography. There is an extra error coming from the $|f\rangle$ state between the two $\pi/2$-pulses in the sixth parity measurement, contributing about 0.5%. All the above sources of error add up to 7.7%, in good agreement with the 91.3% probability of faithfully measuring a positive correlation for an even cat state in Extended Data Fig. 6a. The lower fidelity for an odd cat state is because of the extra qubit T_1 process for the $|e\rangle$ state due to the negative correlation under the same parity readout protocol.

Quantum filter and correlated data. To mitigate the effects due to qubit decoherence, $|f\rangle$ states of the qubit (undesirable states that obscure the parity measurement) and other imperfections in the qubit readout in extracting the parity, we have applied a quantum filter[33,34] that best estimates the photon state parity. We note that the quantum filter is an integration of the quantum stochastic master equation and depends on the measured trajectory. Extended Data Fig. 7 shows the schematic of the quantum filter. This quantum filter at each point in time is realized in two steps: first, a new density matrix $\tilde{\rho}(C_{t+dt})$ is calculated from the best estimation $\rho(C_t)$ at the previous point, based only on the decoherence of the cavity; second, the density matrix $\tilde{\rho}(C_{t+dt})$ gets updated as the best estimation $\rho(C_{t+dt})$ according to Bayes' law, based on the newly acquired knowledge from the current parity measurement. This best estimated density matrix $\rho(C_{t+dt})$ is then used as the input for the next iteration. We have truncated the dimension of the density matrix to $N = 5\bar{n}$, which is large enough to cover all relevant number states. To initialize the density matrix after a displacement $D(\alpha)$, we have set $\rho(t=0) = (1-n_{th})D(\alpha)|0\rangle\langle 0|D^\dagger(\alpha) + n_{th}D(\alpha)|1\rangle\langle 1|D^\dagger(\alpha)$, taking into account the background photon population in the limit $n_{th} \ll 1$.

At time t, the density matrix of the photon state is $\rho(C_t)$, which depends on all previous correlations. At $t + dt$, considering only the decoherence of the cavity, the expected density matrix from free evolution becomes $\tilde{\rho}(C_{t+dt}) = M_{down}\rho(C_t)M_{down}^\dagger + M_{up}\rho(C_t)M_{up}^\dagger + M_{no}\rho(C_t)M_{no}^\dagger$, where $M_{down} = \sqrt{\kappa_{down}dt}a$, $M_{up} = \sqrt{\kappa_{up}dt}a^\dagger$ and $M_{no} = I - \left(M_{down}^\dagger M_{down} + M_{up}^\dagger M_{up}\right)/2$ are the Kraus operators for photon loss, absorption of thermal photons and no jump events, respectively. We have $\kappa_{down} = (n_{th}+1)\kappa$ and $\kappa_{up} = n_{th}\kappa$, and $\kappa = 1/\tau_{tot}$ is the energy decay rate in the cavity under repeated parity measurements. The additional information C_{t+dt} acquired from the parity measurement at $t + dt$ changes the quantum state according to

$$\rho(C_{t+dt}) = \begin{cases} \mathrm{P}(\mathrm{even}|C_{t+dt})\dfrac{\hat{P}_{even}\tilde{\rho}(C_{t+dt})\hat{P}_{even}}{\mathrm{Tr}\left(\hat{P}_{even}\tilde{\rho}(C_{t+dt})\hat{P}_{even}\right)} & \\ \quad + \mathrm{P}(\mathrm{odd}|C_{t+dt})\dfrac{\hat{P}_{odd}\tilde{\rho}(C_{t+dt})\hat{P}_{odd}}{\mathrm{Tr}\left(\hat{P}_{odd}\tilde{\rho}(C_{t+dt})\hat{P}_{odd}\right)} & \text{if } C_{t+dt} \neq 0 \\ \tilde{\rho}(C_{t+dt}) & \text{if } C_{t+dt} = 0 \end{cases} \quad (1)$$

where $\hat{P}_{even}$ and $\hat{P}_{odd}$ are the projectors onto the even and odd manifolds, $\hat{P} = \hat{P}_{even} - \hat{P}_{odd} = e^{i\pi a^\dagger a}$ is the parity operator, and $\mathrm{P}(\mathrm{even}|C_{t+dt})$ and $\mathrm{P}(\mathrm{odd}|C_{t+dt})$ are the respective probabilities of being in the even- and odd-parity manifolds for a measured C_{t+dt}. To simplify the quantum filter, we assume that the event of the qubit jumping to the $|f\rangle$ states is independent of the cavity parity being even or odd. Hence, if the measured correlation is zero, the density matrix of the photon state is assigned to the one expected from free evolution. On the basis of Bayes' law, equation (1) becomes

$$\rho(C_{t+dt}) = \begin{cases} \dfrac{1}{\mathrm{P}(C_{t+dt})}\left(\mathrm{P}(C_{t+dt}|\mathrm{even})\hat{P}_{even}\tilde{\rho}(C_{t+dt})\hat{P}_{even}\right. & \\ \qquad \left. + \mathrm{P}(C_{t+dt}|\mathrm{odd})\hat{P}_{odd}\tilde{\rho}(C_{t+dt})\hat{P}_{odd}\right) & \text{if } C_{t+dt} \neq 0 \\ \tilde{\rho}(C_{t+dt}) & \text{if } C_{t+dt} = 0 \end{cases}$$

where $\mathrm{P}(C_{t+dt}) = \mathrm{P}(C_{t+dt}|\mathrm{even})\mathrm{Tr}\left[\hat{P}_{even}\tilde{\rho}(C_{t+dt})\hat{P}_{even}\right] + \mathrm{P}(C_{t+dt}|\mathrm{odd})\mathrm{Tr}\left[\hat{P}_{odd}\tilde{\rho}(C_{t+dt})\hat{P}_{odd}\right]$. The best parity estimation of the photon state is then

$$P(t+dt) = \mathrm{Tr}\left[\rho(C_{t+dt})\hat{P}\right]$$

This formula has been used extensively in the main text to estimate the parity of the photon state.

To make a comparison with the best parity estimation on the basis of the above quantum filter, we also directly correlate the neighbouring parity measurements without any further processing. For zero correlation cases, because no information of the photon state parity is acquired, the best knowledge of parity at those points is just the last measured non-zero correlation. We assume the repeated parity measurement is a Markovian process. The ensemble-averaged parity dynamics obtained from the correlation under a repeated parity monitoring is then simply

$$\langle C_{cor}(t)\rangle = \mathrm{P}(+1,t) - \mathrm{P}(-1,t) + \mathrm{P}(0,t)\frac{\mathrm{P}(+1,t) - \mathrm{P}(-1,t)}{\mathrm{P}(+1,t) + \mathrm{P}(-1,t)} \quad (2)$$

where $\mathrm{P}(+1,t)$, $\mathrm{P}(-1,t)$ and $\mathrm{P}(0,t)$ are the probabilities of measuring positive, negative and zero correlations at time t, respectively. The third term comes from the fact that the cases with zero correlation are assigned to cases previously measured to have non-zero correlation $+1$ or -1, whose probabilities are respectively $\mathrm{P}(+1,t-dt)$ and $\mathrm{P}(-1,t-dt)$. For small dt, $\mathrm{P}(\pm 1,t-dt) \approx \mathrm{P}(\pm 1,t)$.

The probabilities $\mathrm{P}(+1,t)$, $\mathrm{P}(-1,t)$ and $\mathrm{P}(0,t)$ depend on both the measured parity readout property $\mathrm{P}(\pm 1,0|\mathrm{even/odd})$ and the even and odd parity evolutions, $P_e(t)$ and $P_o(t)$, of the photon state:

$$\mathrm{P}(+1,t) = \mathrm{P}(+1|\mathrm{even})P_e(t) + \mathrm{P}(+1|\mathrm{odd})P_o(t)$$
$$\mathrm{P}(-1,t) = \mathrm{P}(-1|\mathrm{even})P_e(t) + \mathrm{P}(-1|\mathrm{odd})P_o(t)$$
$$\mathrm{P}(0,t) = \mathrm{P}(0|\mathrm{even})P_e(t) + \mathrm{P}(0|\mathrm{odd})P_o(t)$$

where $P_e(t) = \left(e^{-2|\alpha|^2 e^{-\kappa t}} + 1\right)/2$ and $P_o(t) = \left(1 - e^{-2|\alpha|^2 e^{-\kappa t}}\right)/2$.

With all the parameters in equation (2) known, $\langle C_{cor}(t)\rangle$ can be predicted. The agreement with the measured data is excellent, as shown in Extended Data Fig. 8a. This data set is the same as that shown in Fig. 4. Equation (2) even accurately predicts the offset in the averaged parity at $t = 0$, which comes from the asymmetric parity readout fidelities between the even and odd states. The fact that the saturated parity value in the long time limit in Extended Data Fig. 8a is much lower than that in Fig. 4 is mainly a result of the qubit decoherence and the imperfections in the qubit readout. This large difference is additional proof of the effectiveness of the quantum filter. Extended Data Fig. 8b shows a direct comparison between the quantum filtered parity estimation and the direct correlation of qubit states between neighbouring parity measurements. The filtered data are clearly much smoother and can reject the brief changes in the correlated data, directly demonstrating the effectiveness of the quantum filter.

For a coherent state in a thermal bath, its parity dynamics is simply[21]

$$P = \frac{1}{1+2n_{th}}e^{-2|\alpha|^2 e^{-\kappa t}/(1+2n_{th})}$$

which has been used to fit the curves in Fig. 4.

Statistics of photon jumps. To test how faithfully our repeated parity measurement can track photon losses, we simply count the number of jumps extracted from the parity estimator during 500 μs repeated parity measurements. We have applied a Schmitt trigger to digitize the parity estimator to reject the unavoidable noise (spikes in the estimator) coming from qubit decoherence and erroneous parity readout. The two thresholds for the Schmitt trigger are chosen to be ± 0.9 for a large discrimination. Then the number of parity jumps is inferred from the number of transitions in the digital data after the Schmitt trigger.

Although our single parity readout fidelity is about 80% (Extended Data Fig. 6a), owing to the averaging effect of the quantum filter we actually can achieve nearly unity detection sensitivity of single-photon jump events. However, because of the finite bandwidth of the filter, if two photon jumps occur within the response time of the filter τ_f (defined as the time to make a transition between the two thresholds for the Schmitt trigger), our Schmitt trigger will not catch both jumps. Extended Data Fig. 8c shows the time response of the quantum filter applied to typical photon jump events. Green and cyan curves are fits of the parity estimator at the transition based on a hyperbolic tangent function, giving a transition time constant of less than 1 μs. We also find the response time of the filter to make a transition between ± 0.9 to be $\tau_f \approx 2$ μs. The probability of having a second photon jump within τ_f after the first jump is simply $\mathrm{P}_{jump} = \frac{\bar{n}}{\tau_{tot}}\int_0^{\tau_f} e^{-t\bar{n}/\tau_{tot}}dt = 1 - e^{-\tau_f\bar{n}/\tau_{tot}}$. For $\bar{n} = 1$ and $\tau_{tot} = 49$ μs, the above probability is $\mathrm{P}_{jump} = 4\%$, and $\mathrm{P}_{jump} = 15\%$ for $\bar{n} = 4$, which is the probability of missing both jumps.

Extended Data Fig. 9 shows the histograms of the extracted number of jumps for an initial even or odd cat state obtained by post-selection. We note that the almost non-mixing distribution of even and odd numbers is trivial for the following reason. At the end of 500 μs repeated parity measurements, the cavity is already in a steady state with $n_{th} = 0.02$ photons, that is, 98% probability at vacuum (even parity) and 2% probability with one photon (odd parity). When the initial parity of the cat state, for example an even parity, is determined by post-selection, the number of jumps should have 98% probability of being even and only 2% probability of being odd, closely tied with the distribution of the final parity at $t = 500$ μs. A similar argument applies for an initially odd-parity cat state. The even–odd distributions in Extended Data Fig. 9 indeed show a 98-to-2% mixing, providing another way of determining n_{th}.

In reality, we have no way of knowing the true number of photon jumps for each parity measurement trajectory. The only way to test how faithfully our repeated parity measurement can track photon jumps is to see whether the distribution of jumps agrees with what we expect. Owing to the complication of background thermal excitation and the finite response time of the filter, to get an analytic solution is difficult. Instead, we perform a numerical Monte Carlo simulation to compare with the experiment. In the simulation, we use a coherent state as the initial state without distinguishing the parity. Each simulation trajectory is 500 μs long, and includes a transition probability of having a photon enter the cavity to change the photon number from n to $n+1$ as a result of the background thermal excitation. In the simulation, we also neglect those who have neighbouring jumps within the response time τ_f of the quantum filter. Then for each trajectory we count the number of jumps and finally construct a histogram (black solid lines in Extended Data Fig. 9) of those numbers based on 100,000 trajectories. The good agreement between simulation and data demonstrates that the repeated parity measurement can track the error syndromes faithfully.

Quantifying parity-tracking performance. Our demonstrated parity-tracking protocol has several sources of infidelity that lead to a loss of the encoded information in the cat states, ultimately putting a bound on the improvement we would be able to achieve in an actual QEC protocol. This infidelity (Extended Data Fig. 6d) can be broken down into three categories: missed fast photon jumps (due to the limited bandwidth of the measurement), misinterpreted photon jumps (due to qubit T_ϕ and readout inaccuracy), and dephasing of the cat states due to the relaxation of the ancilla qubit during a parity measurement protocol (qubit T_1 process only, as explained later). Missing jumps certainly amounts to a complete loss of phase information. A distinction has to be made between the last two effects because misinterpreting photon jumps need not fully degrade our knowledge of the cavity state's parity at a given point in its trajectory and can be minimized by multiple repeated measurements (discussed more later). Recalling the Wigner tomogram in Fig. 2 aids in appreciating this point. Despite the 80% fidelity of a single parity measurement, after just three of them we can be very confident of the parity of our cavity state, because the probability of having three errant measurements is $(0.2)^3 = 0.8\%$. This is evident when inspecting the behaviour of the quantum filter in the single-shot traces; given three consecutive measurements that are the same, the filter converges to ± 1 with nearly 100% confidence. In the Wigner tomography, this would amount to knowing the value at the origin very well, but, given the cat state dephasing due to qubit T_1, not knowing the full contrast of the fringes and coherent state populations.

To realize the cat states as a quantum memory, the entire state must be preserved in order that an eventual decoding procedure[14] faithfully maps the information back onto some other component (for example a physical qubit). Given the long lifetime of our cavity, an 80% fidelity indicates that a large contribution to an incorrect parity measurement arises from two sources of qubit decoherence: T_1 and T_ϕ. The detrimental effects of T_1 decay are apparent when recalling the entanglement between the cavity and the ancilla qubit, where the cat state begins to acquire a phase at a rate $q\chi_{qs}$ that depends on the qubit state ($|g\rangle$ ($q=0$), $|e\rangle$ ($q=1$), $|f\rangle$ ($q=2$)). Again, the rotating frame has been fixed to be the one rotating at the cavity frequency ω_s when the qubit is in the $|g\rangle$ state. Concretely, if qubit T_1 relaxation happens at t during the parity protocol waiting time π/χ_{qs}, the ideal cat state $(|\alpha\rangle \pm |-\alpha\rangle)/\sqrt{2}$ before the parity measurement will become $\left(|\alpha e^{i\chi_{qs}t}\rangle \pm |-\alpha e^{i\chi_{qs}t}\rangle\right)/\sqrt{2}$. Again, for reasons of simplicity, we have used the approximation $\mathcal{N}_+ = \mathcal{N}_- = 1/\sqrt{2}$ in the large-$|\alpha|$ limit for the rest of Methods. Similarly, during the time between parity measurements, the ideal cat state $(|\alpha\rangle \pm |-\alpha\rangle)/\sqrt{2}$ associated with different qubit states will rotate deterministically at a rate $q\chi_{qs}$. Should the qubit state change at a random time without our knowledge, the cat state will change its rotation rate accordingly, and the phase of the cat state will thus become completely random. In the Wigner tomography, this would manifest itself as a washing out of the cat state's features, where, unlike at the origin, successive measurements can only further reduce the fidelity. Thus, in a given single-shot record, qubit T_1 decay (and, indeed, excitations to higher qubit states) imparts an arbitrary phase on the cat states that would be impossible to recover from without some auxiliary correction protocol.

The contribution of qubit dephasing T_ϕ enters in a subtle, different way. Without loss of generality, let us assume the system is initially in state $(|\alpha\rangle + |-\alpha\rangle)|g\rangle/\sqrt{2}$. The first $\pi/2$-pulse in the parity measurement brings the system to $[(|\alpha\rangle + |-\alpha\rangle)|g\rangle + (|\alpha\rangle + |-\alpha\rangle)|e\rangle]/2$. The above state evolves to $\left[(|\alpha\rangle + |-\alpha\rangle)|g\rangle + \left(|\alpha e^{i\chi_{qs}t}\rangle + |-\alpha e^{i\chi_{qs}t}\rangle\right)|e\rangle\right]/2$, where at time t a random phase flip happens. Consequently, the system becomes $\left[(|\alpha\rangle + |-\alpha\rangle)|g\rangle - \left(|\alpha e^{i\chi_{qs}t}\rangle + |-\alpha e^{i\chi_{qs}t}\rangle\right)|e\rangle\right]/2$ and then keeps evolving in the same way, regardless of the sign change of the term associated with $|e\rangle$. At the end of the π/χ_{qs} evolution, the system becomes a product state again, $(|\alpha\rangle + |-\alpha\rangle)(|g\rangle - |e\rangle)/2$. The second $\pi/2$-pulse just takes the qubit to the other pole on the Bloch sphere, opposite to the case without the phase flip, indicating a 'fake' change in parity. Another way to understand the difference between qubit T_1 and T_ϕ errors is to recall the dispersive interaction between qubit and cavity as formulated in the Hamiltonian in the main text: $(\omega_s - \chi_{qs}|e\rangle\langle e|)a^\dagger a$. Any change of the qubit energy results in a change of the cavity frequency, thereby dephasing the cavity state. A phase flip by contrast does not change the qubit energy, and the cavity phase therefore remains unaffected. Any extra phase acquired by the cavity state contingent on the final qubit state post-measurement would be completely deterministic (to within our ability to discriminate between $|e\rangle$ and $|g\rangle$). We note that the slow drift of the qubit frequency over time can also contribute to cat state dephasing. The cavity frequency change is of the order of $\chi_{qs}df/\Delta$, where df is the qubit frequency change and Δ is the qubit and cavity detuning. With a χ_{qs}/Δ of roughly 1/1,000, and a drift of qubit frequency of the order of 7 μs, we estimate this cavity dephasing to occur on timescales of the order of 10 ms, much longer than any other timescale in our system. Therefore, this source of dephasing can be neglected. To summarize, qubit dephasing thus results in an incorrect parity measurement, but does not impart any erroneous phase onto the cavity state. Instead, by contributing to the 80% fidelity, the effect of T_ϕ necessitates more measurements to achieve a high degree of confidence in the estimation of the cavity state's parity. As increasing the number of measurements increases the likelihood of T_1 decay, qubit dephasing still facilitates an overall degradation of cat state fidelity.

The effective cavity decay rate, κ_{eff}, which predicts the gain one would expect to see in a parity-tracking protocol over the natural cavity photon jump rate $\bar{n}\kappa$, can be described by the sum of all dominant error rates including the three sources of infidelity described above plus a fourth to include readout errors. This κ_{eff} should also be a function of the number of consecutive parity measurements to make, N, and a waiting time τ_W between each one of these N-measurement 'packets' (Extended Data Fig. 10). Quantifying the parity-tracking performance as the foundation for a QEC protocol comes down to finding the optimal N and τ_W that give the lowest κ_{eff}, given the realistic experimental parameters at hand. Explicitly, we have

$$\kappa_{\mathrm{eff}} = \left[\frac{(\bar{n}\kappa)^2(N\tau_M+\tau_W)^2}{2} + N\epsilon_{T_1} + \mathcal{O}\left(\epsilon_{T_\phi}^m\right) + \mathcal{O}\left(\epsilon_M^m\right)\right]\frac{1}{N\tau_M+\tau_W}$$

where τ_M is the time it takes to perform one parity measurement, $\epsilon_{T_1} \approx \tau_M/T_1$, $\epsilon_{T_\phi} = \pi/\chi_{qs}T_\phi$ and ϵ_M are the losses of cat fidelity due to qubit T_1, T_ϕ and measurement inaccuracy, respectively (see section on Wigner tomography above), and $m=(N+1)/2$.

Central to this idea is understanding that incorrect knowledge of the number of parity jumps is the first major contribution to cat state decoherence. Slow photon jump events can be tracked as demonstrated in the main text, and the corresponding phase errors can therefore be completely corrected. This means that single jumps can be tolerated. The term that goes like $(\bar{n}\kappa)^2$ determines the probability of instead having two or more jumps within the time window $N\tau_M+\tau_W$. Measurement infidelity in the form of qubit dephasing ϵ_{T_ϕ} and ϵ_M contributes to misleading the observer that a jump has occurred, which is equivalent to losing track of the number of jumps. These terms contribute to the κ_{eff} expression exponentially, and in a 'majority vote' fashion (assuming N is odd), which explains the choice of exponent in ϵ_{T_ϕ} and ϵ_M. Therefore, in principle the errors due to ϵ_{T_ϕ} and ϵ_M can drop out by either simple majority voting or the more elaborate quantum filtering. Collectively, these three terms correspond to cat state dephasing in the event of the incorrect tabulation of the number of jumps the cat state has undergone during its evolution.

The second major contribution to decoherence, ϵ_{T_1}, comes from cat state dephasing due to T_1. It takes only one qubit decay event within a string of N measurements to completely dephase a cat state, which is why ϵ_{T_1} grows linearly with N. Therefore, an optimal balance needs to be struck between gaining information about photon jumps and dephasing the cavity state by inquiring too frequently. To take an extreme case, we assume for a moment that there is no qubit decoherence and detection inaccuracy, so that ϵ_{T_1}, ϵ_{T_ϕ} and ϵ_M are all zero. In this case, each parity measurement would be perfect and the optimal parameters would thus be $\tau_W = 0$ and $N = 1$. In other words, without the threat of qubit-induced dephasing, the best approach would be to measure as frequently as possible. Conversely, with non-zero qubit decoherence, the longer the cavity lifetime, the more advantageous it would be to have a longer τ_W. Indeed, if $\kappa = 0$ then $\tau_W = \infty$. Should the parity tracking protocol become tolerant of qubit T_1 errors, ϵ_{T_1} would instead grow exponentially like ϵ_{T_ϕ}, because it would amount only to an overall loss of measurement fidelity.

Recalling the 83% fidelity of our Wigner tomography to an ideal cat state, the κ_{eff} derived here indicates that this fidelity does not decrease as 0.83^N, with N the number of parity measurements performed. The latter would be the case only if we were to encode a state, perform tomography on it with 83% fidelity, decode the state, whose fidelity to the initial one would then be reduced by 17%, and then repeat this procedure again and again. Of course this is not what we do. After the initial projection onto a cat state, we proceed with repeated parity measurements, and with each subsequent measurement we actually build up our confidence in the

state. At the same time, however, we pay the price of risking complete dephasing due to qubit decay. Thus, the number 0.83 reflects the amount of information we actually acquire when reconstructing the state through tomography rather than the degree to which the state has been corrupted. The actual corruption is related to how QND the measurement is regarding inducing extra photon loss and cavity state dephasing errors. In the main text, we show the former to be very high at 99.8% per measurement. The latter would be $1-\epsilon_{T_1}\approx 94\%$.

Given our system's parameters, we can quantify what level of improvement we can achieve with the demonstrated parity-tracking protocol over a photon jump rate $\bar{n}\kappa$. As seen in Extended Data Fig. 6d, $\epsilon_{T_1}\approx 6\%$, $\epsilon_{T_\phi}\approx 3\%$ and $\epsilon_M\approx 1\%$ are all of the same order. Here we attribute a greater contribution of ϵ_{T_1} from that listed in Extended Data Fig. 6d because the sources of error there assumed that the final qubit state after each measurement was $|g\rangle$. However, without any post-selection of trajectories, the qubit could just as well end up in $|e\rangle$, enhancing the effect of qubit-induced dephasing. Therefore, the optimal N in our case is actually $N=1$, notwithstanding the 80% fidelity of a single parity measurement. This can be understood by noting that for $N>1$, the contribution of ϵ_{T_1} quickly begins to outweigh any qubit dephasing and measurement errors, leading to a suboptimal choice of parameters. Given that the contributions of these terms together sum to about a 10% error, we now have

$$\kappa_{\mathrm{eff}}=\left[\frac{(\bar{n}\kappa)^2(\tau_{\mathrm{M}}+\tau_{\mathrm{W}})^2}{2}+0.1\right]\frac{1}{\tau_{\mathrm{M}}+\tau_{\mathrm{W}}}$$

The minimum κ_{eff} is achieved when the decay rates are equal:

$$(\tau_{\mathrm{M}}+\tau_{\mathrm{W}})^2=\frac{2(0.1)}{(\bar{n}\kappa)^2}\quad\Rightarrow\quad\kappa_{\mathrm{eff}}=\bar{n}\kappa\sqrt{0.2}$$

The improvement over $\bar{n}\kappa$ is thus of the order of $\sqrt{0.2}$, which predicts an improvement in the effective cavity decay time by a factor of two over $1/\bar{n}\kappa$. The corresponding τ_{W} value is 4.6 μs. Given that τ_{M} is dominated in large part by the parity protocol waiting time π/χ_{qs}, a relevant benchmark for the overall performance becomes the product $\chi_{\mathrm{qs}}T_1$. We emphasize that even for this system's modest coherence properties, an improvement by a factor of two would be impressive. Indeed, if T_1 and T_ϕ approach 20 μs, the protected lifetime of the information would exceed 50 μs, the lifetime of a single-photon Fock state in the storage cavity.

The highly QND nature of the parity measurements at 99.8%, expanded on in the main text, was omitted from the analysis above owing to its minor contribution relative to all other sources of error. We consider this number to be one of the two figures of merit for the success of the parity-tracking protocol. If the very act of measuring parity were to induce photon jumps without our knowledge, the parity-tracking protocol itself would be flawed. This success, however, belies the degree to which we perturb the information stored in the cat states. Referring once more the Wigner tomograms, although we can confidently claim that we are QND as far as the point at the origin is concerned, given low qubit T_1 the same cannot be said of the rest of the information present in the Wigner tomogram at other points in I–Q space. In other words, the parity monitoring does not change photon number probabilities, but could change the relative phases between constituent Fock states. This second figure of merit, which can again be quantified as the contribution to cavity state dephasing due to qubit decay ($1-\epsilon_{T_1}\approx 94\%$ per measurement) still clearly leaves much room for improvement. Nonetheless, although certainly presenting challenges, shortcomings arising from qubit performance and other higher-order mechanisms of dephasing not discussed here (such as self-Kerr of the cavity and cross-Kerr due to readout) do not seem insurmountable[35]. Addressing the issue of cavity state dephasing due to measurement is an important next step in improving the performance of this QEC scheme. We are confident that we can address the issue of qubit T_1 without substantially altering the parity-tracking protocol presented here, but we feel that this lies beyond the scope of this work.

31. Siddiqi, I. *et al.* Direct observation of dynamical bifurcation between two driven oscillation states of a Josephson junction. *Phys. Rev. Lett.* **94,** 027005 (2005).
32. Vijay, R., Devoret, M. H. & Siddiqi, I. The Josephson bifurcation amplifier. *Rev. Sci. Instrum.* **80,** 111101 (2009).
33. Belavkin, V. P. Quantum stochastic calculus and quantum nonlinear filtering. *J. Multivariate Anal.* **42,** 171–201 (1992).
34. Bouten, L., van Handel, R. & James, M. An introduction to quantum filtering. *SIAM J. Contr. Optim.* **46,** 2199–2241 (2007).
35. Mirrahimi, M. *et al.* Dynamically protected cat-qubits: a new paradigm for universal quantum computation. *New J. Phys.* **16,** 045014 (2014).

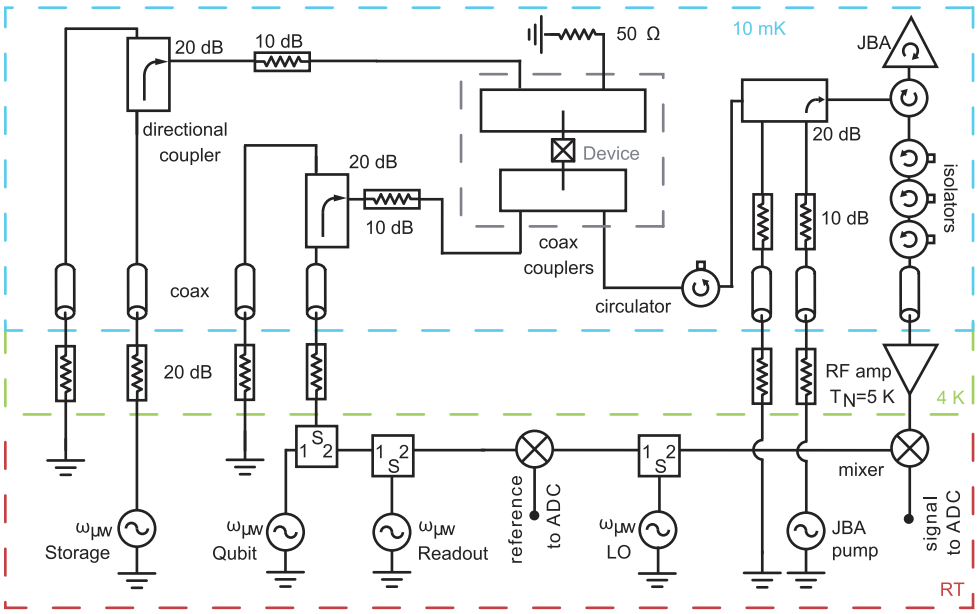

Extended Data Figure 1 | Schematic of the measurement set-up. We use two separate lines to drive the readout and the storage cavity. Qubit state manipulations are realized through the readout cavity input line. The readout cavity output signal is first amplified by a JBA operating in a double-pumped mode, and the reflected signal then goes through three isolators in series before being further amplified by a HEMT at 4 K. The amplified signal is finally down-converted to 50 MHz and then digitized by a fast 1 GS data-acquisition card.

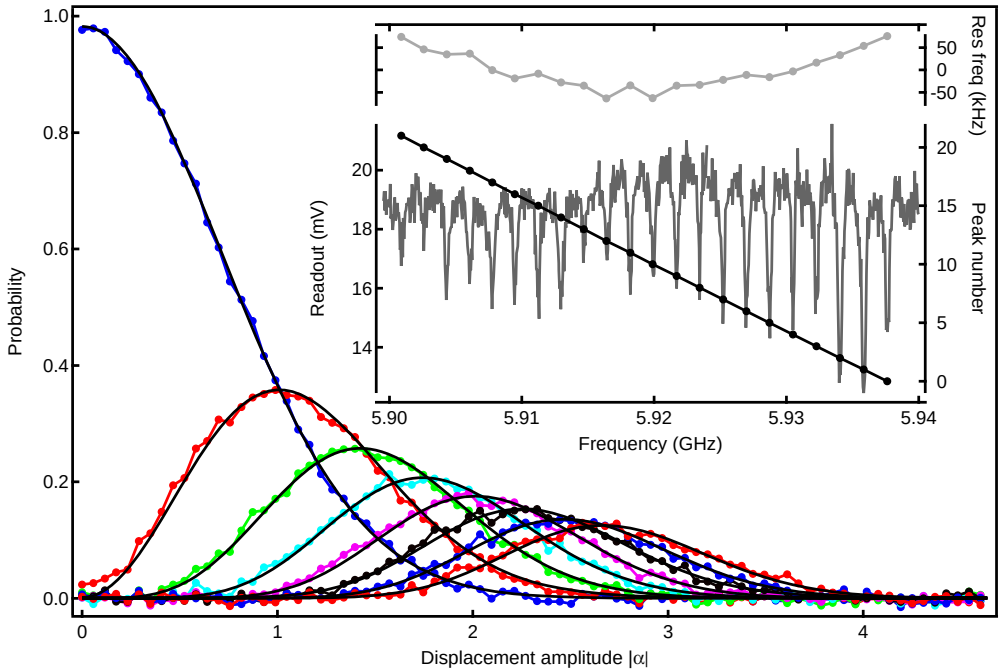

Extended Data Figure 2 | Poisson distribution of photon numbers in the cavity. Dotted colour lines are data for the first eight Fock states $n = 0, 1, 2, \ldots, 7$ as functions of displacement amplitude $|\alpha|$. The measurements are performed with a selective π-pulse on each number splitting peak, and the resulting signal amplitude should be proportional to the corresponding number population. These oscillation amplitudes have been normalized to probabilities such that the sum of the amplitudes corresponding to $n = 0$ and $n = 1$ equals unity. Dashed lines are theoretical curves with a Poisson distribution $P(|\alpha|,n) = |\alpha|^{2n} e^{-|\alpha|^2} / n!$, where the x axis has had a single scale factor adjusted to fit all these probabilities. The excellent agreement indicates good control of the coherent state in the cavity and also gives a good calibration of the cavity displacement amplitude. On the basis of the probability of $n = 1$ at $|\alpha| = 0$, we find a background photon population of $n_{th} = 0.02$ in the cavity. Inset bottom panel: spectroscopy (left axis) of the number splitting peaks of the qubit when populating different photon numbers in the cavity. Inset top panel: difference between peak positions and a linear fit. The curvature necessitates a second-order polynomial fit, resulting in a linear dispersive shift $\chi_{qs}/2\pi = 1.789 \pm 0.002$ MHz and a nonlinear dispersive shift $\chi'_{qs}/2\pi = 1.9 \pm 0.1$ kHz.

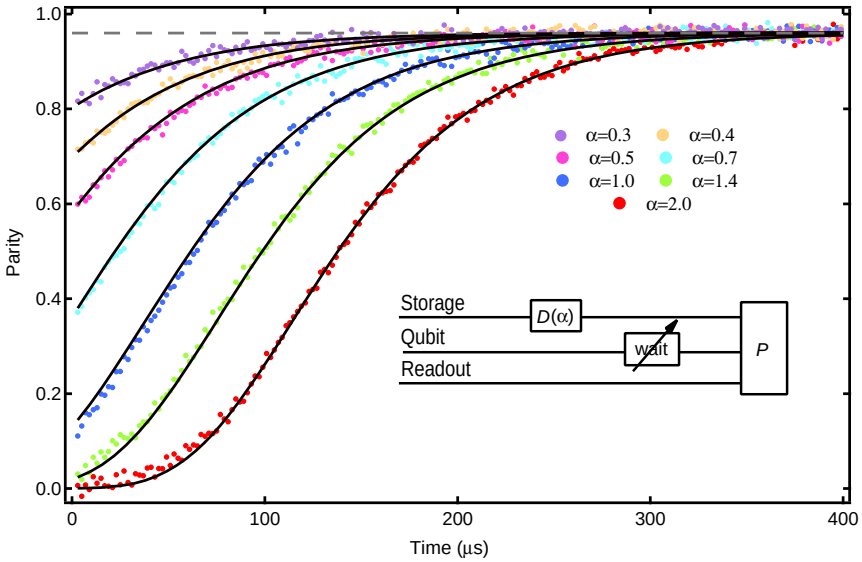

Extended Data Figure 3 | Ensemble-averaged free parity evolution of a coherent state. The measurement protocol is shown in the inset. The single parity measurement gives a readout voltage that has been converted to parity through thresholding. All measured evolution curves saturate at the same value in the long time limit. This saturation level has been forced to 0.96 (because $n_{\mathrm{th}} = 0.02$), represented by the dashed horizontal line. The solid lines are global fits, giving a time constant of $\tau_0 = 55\ \mu\mathrm{s}$.

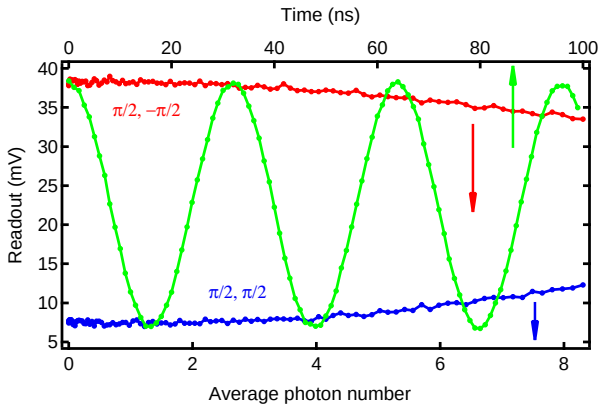

Extended Data Figure 4 | Effectiveness of the $R_{\hat{y},\pm\pi/2}$ pulse. Blue and red data (bottom axis) are ensemble-averaged qubit readouts after consecutively (with no wait time) applying $(R_{\hat{y},\pi/2}, R_{\hat{y},\pi/2})$ and $(R_{\hat{y},\pi/2}, R_{\hat{y},-\pi/2})$, respectively, as functions of different $\bar{n}$ introduced into the cavity. The curvature for $\bar{n} > 4$ comes from the finite bandwidth of the pulses in the frequency domain. Green curve (top axis) is a time Rabi trace for an amplitude comparison with no initial cavity displacement.

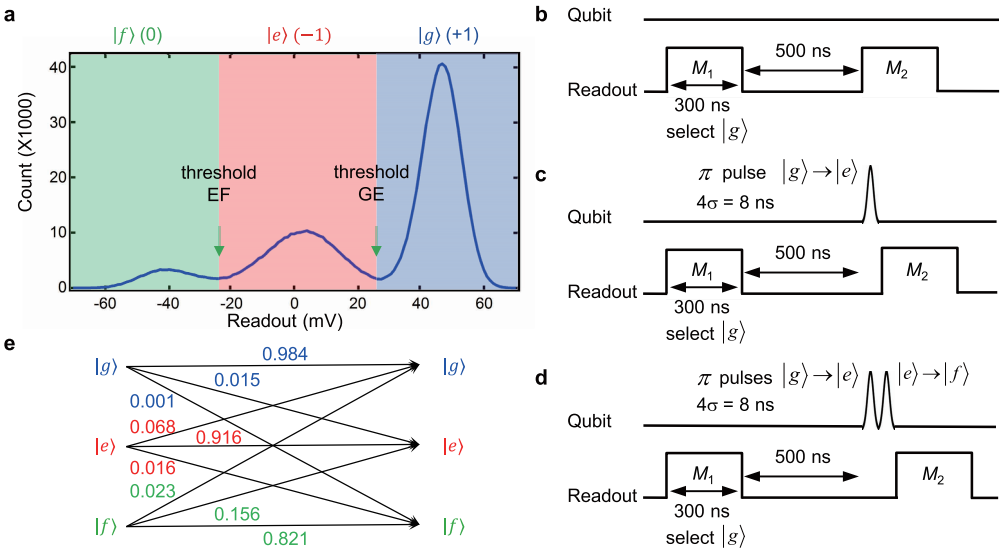

Extended Data Figure 5 | Qubit readout properties. **a**, Histogram of qubit readout for the parity protocol used in repeated single-shot traces in Fig. 3. The phase between the JBA readout and the pump has been adjusted such that |g⟩, |e⟩ and |f⟩ states can be distinguished with optimal spacings. Thresholds between |g⟩ and |e⟩, and between |e⟩ and |f⟩, have been chosen to digitize the readout signal to +1, −1 and 0 for |g⟩, |e⟩ and |f⟩, respectively. Note that we assign a zero to the |f⟩ states to indicate a 'failed' measurement with no useful information about the parity. **b**–**d**, Illustrations of pulse sequences (not to scale) producing the readout error matrix with the storage cavity left in vacuum. The |g⟩ state (**b**) is prepared through post-selection of an initial qubit measurement M_1, whereas |e⟩ (**c**) and |f⟩ (**d**) are prepared by properly pulsing the selected |g⟩ state. A histogram of the second measurement, M_2, gives the qubit readout properties. **e**, Qubit readout properties for qubit initially in |g⟩, |e⟩ and |f⟩, respectively.

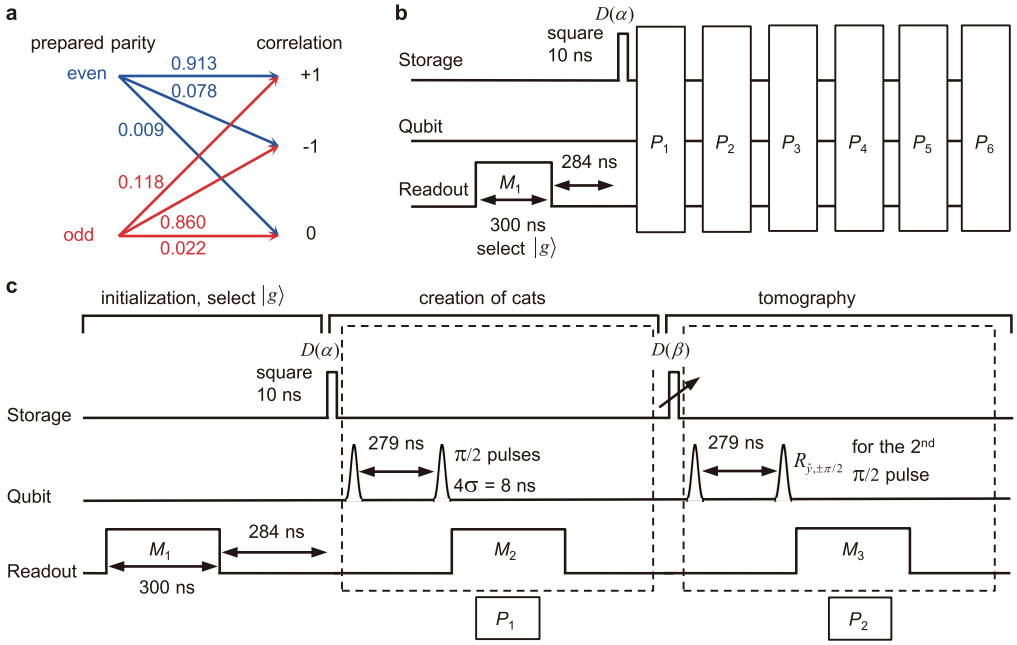

d

source of errors	duration (μs)	coherence time (μs)	contribution to Winger tomography errors
qubit T_1 between two π/2 pulses in P_1	0.28	8.0	3.0%
qubit T_ϕ between two π/2 pulses in P_1	0.28	7.3	3.8%
photon jump between two π/2 pulses in P_1 ($\bar{n}$=4)	0.28	50/ $\bar{n}$ =12.5	1.1%
photon jump during *M2* and waiting time in P_1 ($\bar{n}$=4)	0.58	50/ $\bar{n}$ =12.5	4.6%
photon jump in P_2 ($\bar{n}$=4)	0.28	50/ $\bar{n}$ =12.5	2.2%
qubit measurement inaccuracy in P_1	NA	NA	0.8%
qubit transition up after measuring $\|g\rangle$ in P_1	0.28	56	0.5%

e

source of errors	duration (μs)	coherence time (μs)	contribution to parity measurement errors
qubit T_1 between two π/2 pulses	0.28	8.0	1.8%
qubit T_ϕ between two π/2 pulses	0.28	7.3	3.8%
photon jump between two π/2 pulses ($\bar{n}$=1)	0.28	50	0.3%
qubit measurement inaccuracy in P_5	NA	NA	0.8%
qubit transition up after measuring $\|g\rangle$ in P_5	0.28	56	0.5%
qubit $\|f\rangle$ state	0.28	56	0.5%

Extended Data Figure 6 | Parity readout properties and Wigner tomography. a, Parity readout property for given even and odd parity states for the protocol ($R_{\hat{y},-\pi/2}$ as the second qubit pulse) used in the single-shot traces in Fig. 3 ($\bar{n}=1$). **b**, Protocol to measure parity readout fidelity. An initial qubit measurement allows a post-selection of the $|g\rangle$ state of the qubit, followed by six consecutive parity measurements. The pulse sequence of each parity measurement is shown in P_1 in **c**. P($\pm$1,0|even/odd) are determined by post-selecting the cases with the first five consecutive identical parity results, which give the photon state parity with good confidence, and then constructing a histogram for the sixth parity measurement. **c**, Illustration of pulse sequence (not to scale) for producing the cat states and the Wigner tomography shown in Fig. 2. The protocol starts with a post-selection of the $|g\rangle$ state of the qubit through an initial qubit measurement M_1. A parity measurement is performed immediately after a storage cavity displacement α, followed by Wigner tomography with varying displacements β. A 280 ns waiting time after each measurement has been chosen to ensure that the readout cavity is in the vacuum state. The qubit pulses have a Gaussian envelope truncated to $4\sigma = 8$ ns, and the displacement pulses on the storage cavity are 10 ns square pulses. The dashed enclosures represent the pulse sequences for parity measurement. **d**, Error budgets for Wigner tomography fidelity. **e**, Error budgets for the parity readout fidelities with $R_{\hat{y},-\pi/2}$ as the second qubit pulse.

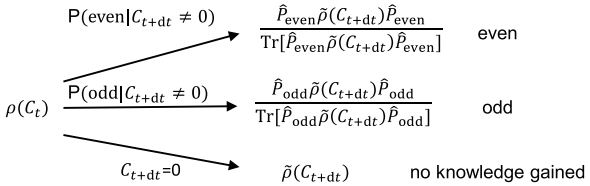

Extended Data Figure 7 | Schematic of the quantum filter. At time t, the density matrix of the photon state is $\rho(C_t)$, which depends on all previous correlations. At $t + dt$, only considering the decoherence of the cavity, the expected density matrix from free evolution becomes $\tilde{\rho}(C_{t+dt})$. The additional information C_{t+dt} acquired from the parity measurement at $t + dt$ changes the knowledge of the parity of the photon state according to equation (1).

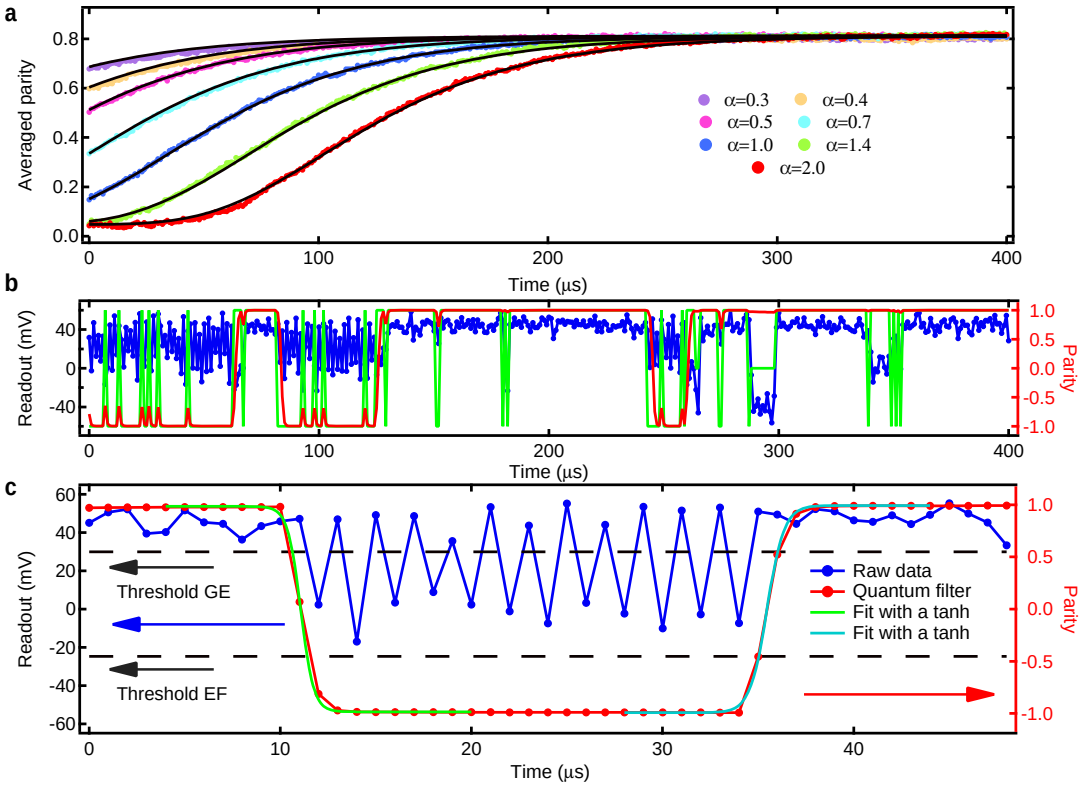

Extended Data Figure 8 | Effectiveness and response time of the quantum filter. **a**, Ensemble-averaged parity dynamics obtained directly from the correlation of qubit states between neighbouring parity measurements. The data set is the same as that shown in Fig. 4. Solid lines are predictions based on equation (2), in excellent agreement with the measured data. The offset of the averaged parity at $t = 0$ comes from the asymmetry between the parity readout fidelities of the even and odd states. The fact that the saturated parity value in the long time limit is much lower than that in Fig. 4 is additional proof of the effectiveness of the quantum filter. **b**, Effectiveness of the quantum filter. Blue (raw) and red (filtered) curves are the same as those shown in Fig. 3e. The green curve is the direct correlation of qubit states between neighbouring parity measurements. The red curve is clearly much smoother and can reject the brief changes in the green curve. **c**, Response time of the quantum filter applied to typical photon jump events. The blue curve is the raw data from a repeated parity measurement. The red curve is the corresponding parity estimator based on the quantum filter. Green and cyan curves are fits to tanh functions of the parity estimator at the transitions down and up, respectively, giving a transition time constant of less than 1 μs. However, the response time of the filter to make a transition between -0.9 and $+0.9$ is $\tau_f \approx 2$ μs.

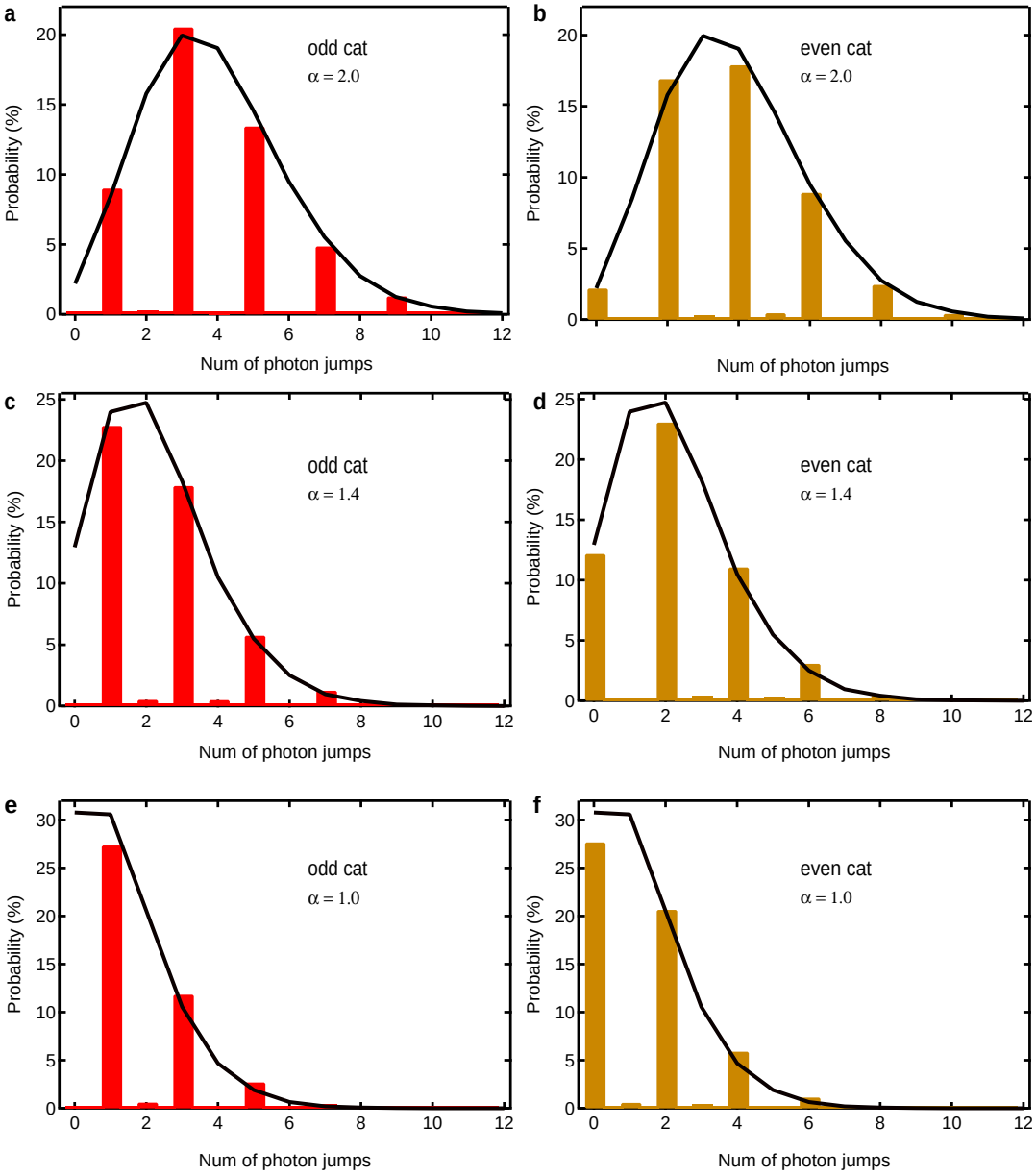

Extended Data Figure 9 | Histograms of the number of jumps extracted from the parity estimator during 500 μs repeated parity measurements for an initial even or odd cat state by post-selection. a, **b**, $|\alpha| = 2.0$; **c**, **d**, $|\alpha| = 1.4$; **e**, **f**, $|\alpha| = 1.0$. Solid lines are numerical simulations including the background thermal excitation and finite response time of the quantum filter. In the simulation, we use a coherent state as the initial state without distinguishing the parity. The good agreement between data and simulation demonstrates that the repeated parity measurement can track the error syndromes faithfully.

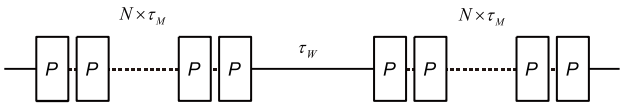

Extended Data Figure 10 | An optimized parity-tracking scheme would involve performing packets of N measurements, each lasting a time τ_M, followed by a waiting time of τ_W.